

**CORRELATION ANALYSIS OF 2D TOMOGRAPHIC IMAGES FOR FLAW
DETECTION IN PAVEMENTS**

Submitted to ASTM Journal of Testing and Evaluation

This paper should be cited as follows:

Hoegh, K., Khazanovich, L., "Correlation Analysis of 2D Tomographic Images for Flaw Detection in Pavements." ASTM International. Journal of Testing and Evaluation. Volume 40. Issue 2. March 2012.

By

Kyle Hoegh

Graduate Research Assistant
Department of Civil Engineering
500 Pillsbury Drive S.E.
Minneapolis, MN 55455-0116
Phone: (507) 398-2669
Email: hoeg0021@umn.edu

Lev Khazanovich

Associate Professor
Department of Civil Engineering
500 Pillsbury Drive S.E.
Minneapolis, MN 55455-0116
Phone: (612)624-4764
Fax: (612)626-7750
Email: khaza001@umn.edu

CORRELATION ANALYSIS OF 2D TOMOGRAPHIC IMAGES FOR FLAW DETECTION IN PAVEMENTS

Kyle Hoegh¹ and Lev Khazanovich²

ABSTRACT

Ultrasonic tomography is an emerging method of non destructive concrete pavement diagnostics which can be used for improved quality assurance/quality control during concrete pavement construction and assist in rehabilitation decision making. Detection of flaws using ultrasonic tomography requires significant effort and user expertise. To address these limitations, a quantitative method for determining the presence of defects in concrete pavements was developed. The proposed method is an adaptation of the recently developed impact-echo signature analysis method (IESA), which is used for comparison of impact-echo signals. The proposed two-dimensional ultrasonic tomography signature analysis (2D-UTSA) method was used to compare two-dimensional B-scans obtained using a commercial test system in field trials at the Minnesota Road Research Facility and the Federal Aviation Administration's National Airport Pavement Test Facility. Analysis of the results showed that the 2D-UTSA method is capable of identifying subsurface defects.

¹Graduate Research Assistant, Department of Civil Engineering, The University of Minnesota, Minneapolis, MN 55455-0116, (corresponding author). Email: hoeg0021@umn.edu

²Associate Professor, Department of Civil Engineering, The University of Minnesota, Minneapolis, MN 55455-0116, Email: khaza001@umn.edu

Keywords: ndt, infrastructure, airport pavement, ASR, diagnostics, delamination, deterioration

INTRODUCTION

Non destructive testing (NDT) techniques, such as ground penetrating radar (GPR), magnetic field tomography, infrared thermography, sounding, and stress wave methods, have been used to evaluate concrete pavements for many years. All of these methods are based on different physical principles and have unique strengths and limitations.

GPR transmits electromagnetic waves into the test medium and the reflection of those waves at interfaces of different dielectric properties gives information about changes in the test medium. The wave speed is dependent on the dielectric properties of the material, and can be used to determine the target depth. Past studies have shown that GPR is capable of achieving high speed measurements of thickness and pavement distress such as delamination, although the accuracy reduces with higher speeds and detection of non-uniform cracks is difficult [1-5].

Magnetic techniques use magnetic pulse-induction and the distribution of the eddy current induced by an applied magnetic field to determine the position, size, shape, and orientation of metal inclusion in a pavement. Numerous evaluations of the accuracy of one of magnetic pulse-induction device, the MIT Scan-2, have shown it to be a reliable tool for locating metal inclusions with high accuracy. It should be noted that this method does not detect any type of non-metallic inclusions or defects [6-8].

Infrared thermography can detect thermal anomalies by measuring infrared emission at the surface of a pavement. A difference in surface temperature can indicate a subsurface anomaly such as the presence of delamination in concrete, although this method is limited by environmental conditions and depth of the defect [9-11].

This paper explores the use of ultrasound techniques, specifically the state-of-the-art ultrasonic tomography device MIRA, for concrete pavement evaluation. Ultrasonic testing uses high frequency (greater than 20,000 Hz) stress waves to characterize the properties of

materials or to detect hidden defects. Stress waves generated by transducers travel through the material and are reflected back to the surface at interfaces when they encounter a change in acoustic impedance (e.g. concrete to air). The reflected waves are received at the surface and analyzed to provide information about the media through which the stress waves propagated.

Ultrasonic measurement and imaging techniques have been used successfully for many years in biomedical applications and for flaw analysis in both metals and composite materials [12, 13]. However, earlier applications of ultrasonic technology for the evaluation of Portland cement concrete (PCC) have experienced difficulties due to the heterogeneous nature of the material. Previous ultrasonic methods for testing concrete structures relied on a time consuming liquid coupling process. In addition, ultrasound frequencies in the MHz range typically used for steel structures and in medical applications do not penetrate to a great enough depth for concrete diagnostics due to the excessive attenuation of the wavefront caused by the heterogeneity of the concrete[14]. These difficulties create serious impediments to wider use of ultrasonic testing for the evaluation of concrete structures.

Evaluation of pavements and bridge decks for delaminations or other internal conditions is commonly conducted through chain dragging. However, this method is not effective in determining the precise location and extent of damage [5]. Additionally, it is difficult to cover large areas and chain dragging is highly dependent on the expertise of the operator, making the evaluation very subjective. Conventional impact echo (IE) is a more sophisticated and accurate acoustical method which can be used in place of chain dragging. IE is capable of detecting planar layer interfaces, which can be used for thickness determination or the detection of other plate-like inclusions. Testing with this method is time consuming and only allows for one signal pair to be sent and received per scan. With only one mechanical impact signal and analysis methods that require multiple reflections at the

same boundary using frequency domain analysis, there are difficulties in evaluating the complex geometries required for irregular flaw detection. [5, 14-16]. Improved techniques, such as air coupled impact echo, have been developed to allow for more productive measurements and multiple measurement pairs [17-19].

The ultrasonic tomography method presented in this paper eliminates some of the issues associated with other techniques used to detect flaws in concrete pavements. One improvement is the use of dry point contact (DPC) transducers, which eliminates the issues associated with using liquid couples and only one signal. The dry point contact is possible due to the small size of the contact zone of each transducer (less than 1-2 mm [0.04 in.-0.08]). For this small of a contact zone, the transducer produces an oscillating force that can be treated as a point force. In this case, a contact liquid couple is not required for transmission of the shear wave to the tested medium [20].

The transducers have been developed with the capability of transmitting relatively low frequency (55 khz) shear waves to penetrate to the necessary depths without relying on liquid coupling [20-22]. Each transducer consists of two parallel piezoelectric elements surrounded by a liquid composite material. The transducer can be used as a transmitter or receiver. Each transmitting-receiving pair radiates and receives a transformable short duration shear wave impulse. The shear wave impulses are generated by oscillating the piezo-elements at a 180 degree time lag (antiphase). Self reverberation noise is kept to a low level by damping with a liquid composite material that surrounds the piezo-elements [20].

Use of these transducers allows for a multiple measurement pairs in each scan, and has been successfully applied for over a decade to detailed evaluation of civil structures [15, 21, 23-25]. The development of these transducers and the availability of powerful computers led to the introduction of an ultrasonic tomography device, MIRA, for diagnostics of concrete structures [26]. MIRA incorporates 10 channels, each composed of four transmitting and

receiving transducers in a linear array. This linear array operates in a multi-static nature, allowing for 45 transmitting and receiving pair time-of-flight measurements (see Figure 1) in less than three seconds. The spacing between adjacent transducer channels is 40 mm (1.6 in.). Thus, horizontally spaced measurement pairs in each MIRA scan include nine pairs at 40 mm (1.6 in.) spacing, eight pairs at 80 mm (3.1 in.) spacing, seven pairs at 120 mm (4.7 in.) spacing, six pairs at 160 mm (6.3 in.) spacing, five pairs at 200 mm (7.9 in.) spacing, four pairs at 240 mm (9.4 in.) spacing, three pairs at 280 mm (11.0 in.) spacing, two pairs at 320 mm (12.6 in.) spacing and one pair at 360 mm (14.2 in.) spacing.

The data obtained from the transducers is processed using the Synthetic Aperture Focusing Technique (SAFT) to produce an image called a SAFT B-scan, which gives a visual representation of the cross section of the scanned area. The SAFT B-scan process used by MIRA has a few differences compared to conventional IE analysis, including use of shear waves rather than compression waves, time domain analysis rather than frequency domain, and image reconstruction from multiple measurement pairs rather than a single point result from one measurement pair.

The DPC transducers provide the necessary consistency in shear wave pulses and wavefront penetration required for diagnostics at depths up to 3 ft. (0.914 m). The use of multiple sensor pairs for each scan give the required redundancy of information necessary to evaluate a heterogeneous media such as Portland cement concrete (PCC) [27]. On the right side of Figure 1, the increased redundancy of information of MIRA (bottom) over conventional IE (top) can be observed, where the multi-static linear array of transmitting and receiving transducers creates 45 measurement angle pairs, compared to one measurement pair obtained in traditional IE. The increased redundancy of information allows for time domain analysis such as the SAFT B-scan, rather than resonance of multiple reflections at one point. This time-of-flight analysis with multiple incident angles can assist in evaluating more

complex geometries, where non-planar flaws may not result in resonance of multiple reflections at the interface, as would be the case using conventional IE.

The left side of Figure 1 shows a MIRA measurement in progress, in which the transducers are placed flush with the surface for generating a SAFT B-scan. A B-scan is a two dimensional reconstruction of reflecting interfaces in the concrete directly below the array of transducers, with high intensity areas indicating strong reflections due to changes in acoustic impedance. Each pixel location in the B-scan is associated with a physical location (depth and lateral position below the array of transducers). In the tomograph, each applied grayscale shade indicates the intensity of reflection values, as computed by the SAFT algorithm based on the location of the sending and receiving transducers, measured velocity, and time-of-flight. The short pulse transmitted by the transducers allows for more precise calculation of the locations causing reflections for each measurement pair. Since the basic premise of SAFT is to use superposition to combine the high intensity of reflection areas caused by flaws or any change in acoustic impedance in the various 45 transmitting-receiving pairs, it is important to have a small duration (short pulse) of the high intensity reflected areas for more precise superposition.

Figure 2 shows an example SAFT B-scan taken in sound concrete. In each SAFT B-scan, the horizontal axis represents the location (mm) along the aperture of MIRA with 0 at the center of the transducer array and the vertical axis indicates the depth (mm) below where the scan was taken. Within B-scans, any change in acoustic impedance (i.e., from concrete to air, concrete to metal, or concrete to a base) results in a high intensity image (black), while areas of through transmission (i.e. sound concrete) are indicated by a low intensity image (white) [26]. It can be observed from Figure 2 that there is an area of higher intensity where there is an interface between the concrete and base at a depth of about 600 mm. It should be

noted that the SAFT tomographic reconstruction can also be applied to other multiple transmitting-receiving pair measurements with the capability of emitting short pulses [25].

While manual analysis of these B-scans can be a powerful tool for evaluating subsurface defects in concrete, it can be very time consuming and is dependent on user expertise. These factors become an issue when evaluating a large amount of collected data, where the results of testing are needed before each B-scan can be manually analyzed. A shape recognition method of automating the analysis of concrete cover over reinforcement in PCC has been developed to reduce the analysis time [27]. In the case study outlining the advantages of the automated analysis for that problem, the analysis time of 3 miles (4.8 km) of pavement testing was reduced from a few weeks to a few hours. However, there is no such automated method for detection of irregular defects in concrete. The method proposed in this paper allows for an initial rapid screening that can identify areas of interest for further manual evaluation. This will reduce the need to manually analyze every scan, which will significantly reduce the analysis time for large scale projects where concrete defect identification is necessary. Because information about the type of defect or location within the scan is lost in the method, it should only be used as a filtering method to assist in determination of locations where defects are present. The type of manual B-scan analysis presented by Hoegh et al. [27] can then be used to determine the type and location of the defect within the area of interest.

PAST EXPERIMENTAL STUDIES

Previously, identification of reinforcement location in concrete from MIRA B-scans has been automated using shape recognition techniques [27]. This method was feasible because the geometry of the reinforcement was known within each scan and in relation to adjacent scans. However, improper concrete consolidation and other flaws are generally non-uniform

and *a priori* knowledge of the reflector type and dimension is not available. Automated detection of these types of defects, which are stochastic in nature, requires a method that does not rely on shape recognition.

Recently Schubert and Koehler have applied impact-echo signature analysis (IESA) for the evaluation of the grouting conditions in bridge deck tendon-ducts [15]. IESA utilizes Pearson's correlation for comparison of one-dimensional (1D) impact-echo signals with a reference signal in either the time or frequency domain. For time domain analysis, Equation 1 shows the Pearson's correlation equation which was used for comparison of 1D impact-echo signals [15]:

$$C_{XY}^j = \frac{Cov[X, Y^j]}{\sqrt{Var[X]Var[Y^j]}} = \frac{\sum_{i=1}^N (x_i - x_{mean})(y_i^j - y_{mean}^j)}{\sum_{i=1}^N (x_i - x_{mean})^2 \sum_{i=1}^N (y_i^j - y_{mean}^j)^2} \quad (1)$$

Where j is the j -th signal, i is the i -th intensity value within a signal, X and Y^j are the intensity amplitude vectors of the reference and j -th IE scans, respectively; Cov and Var stand for the covariance and variance; x_i is the i -th intensity value within the reference signal and y_i is the i -th intensity value within the current signal, respectively; x_{mean} and y_{mean}^j are the mean intensity of the reference signal and current signal, respectively; N is the number of intensity values in each signal being compared; and C_{XY}^j is Pearson's correlation coefficient, which measures the strength of the linear dependence between IE intensity measurements X and Y^j . Thus, a C_{XY}^j value of 0 would indicate no correlation, higher C_{XY}^j values indicate similar signals, and a C_{XY}^j value of one indicates that the two signals are related linearly.

Using Equation 1, a correlogram can be constructed of the correlation coefficients associated with each measurement location. By quantifying the similarity of the signal at each location with a reference acoustic signature representing a "damage-free" position, areas with low correlation coefficients would indicate the presence of scatterers. Through analysis

of numerically simulated and laboratory test data, Schubert and Koehler concluded that the IESA method is an ideal extension to traditional evaluation procedures based on stationary reflections or resonances by large planar flaws. Figure 3 shows an example correlogram, where a dip in Pearson's correlation can be observed at the three simulated inclusions of a concrete plate.

Schubert and Koehler also stated that *a priori* knowledge of a reference signal where no scatterers are present is not generally available. Further, they concluded that a 1D waveform is susceptible to misinterpretations [15]. One potential misinterpretation when using this method is improper selection of the reference signal. When evaluating 1D waveforms, it can be difficult to differentiate the reflection amplitude levels caused by actual defects in the concrete from structural noise which can be caused by different aggregate types and air void distributions. It is proposed to generalize the IESA method for use with SAFT B-scan reconstructions that are obtained from MIRA or other tomography reconstructions. The reference signal issue is also considered.

ULTRASONIC TOMOGRAPHY SIGNATURE ANALYSIS

The IESA method can be generalized into a two dimensional ultrasonic tomography signature analysis method (2D-UTSA) for evaluation of SAFT B-scans. Pearson's correlation coefficient is adapted for comparison of reconstructed intensity matrices from SAFT B-scans such as that shown in Figure 2 as follows:

$$C_{XY_{2D}}^j = \frac{Cov[X_{2D}, Y_{2D}^j]}{\sqrt{Var[X_{2D}]Var[Y_{2D}^j]}} = \frac{\sum_{i=1}^N \sum_{k=1}^M (x_{ik} - x_{2Dmean})(y_{ik}^j - y_{2Dmean}^j)}{\sum_{i=1}^N \sum_{k=1}^M (x_{ik} - x_{2Dmean})^2 \sum_{i=1}^N \sum_{k=1}^M (y_{ik}^j - y_{2Dmean}^j)^2} \quad (2)$$

where X_{2D} and Y_{2D}^j are the matrices of reflection intensity for the reference B-scan and current B-scan, respectively; x_{ik} and y_{ik}^j are the single intensity values of the reference signal

and current signal, respectively, with depth below the measurement location increasing with i and the location along the aperture of the scan increasing with k ; X_{2Dmean} and Y_{2Dmean}^j are the mean intensities of the reference B-scan and current B-scan, respectively; N and M are the number of intensity values in the depth and device aperture direction, respectively; and C_{XY2D}^j is Pearson's correlation coefficient, which measures the strength of the linear dependence between X_{2D} and Y_{2D}^j .

Thus, if a SAFT B-scan taken on relatively sound concrete with similar structural geometry is used as the reference scan, flawed concrete locations can be identified. On the extremes, a C_{XY2D}^j value of 0 would indicate no correlation and a C_{XY2D}^j value of 1 would indicate that the two B-scans are related linearly. Therefore, a higher C_{XY2D}^j would indicate similar scans or sound concrete, and a significant decrease in the correlation coefficient would indicate dissimilar B-scans, or flawed concrete, especially if observed in a group of adjacent scans. This type of analysis will be referred to as the 2D-UTSA method.

In addition to making the method applicable for the type of data gathered by MIRA, the use of the expanded Pearson's correlation for 2D comparison improves the method by correcting the issues of the IESA technique in selecting the reference signal. In the SAFT B-scan reconstruction process, natural variation in reflection amplitude within each of the 45 transmitting-receiving transducer pairs cancels out, while reflection amplitudes caused by interfaces where there is a change in acoustic impedance combine. Conversely, natural variation can significantly affect comparison of one transmitting/receiving pair. Because each scan is a reconstruction based on 45 transmitting-receiving transducer pairs, this added redundancy reduces the chances of misinterpretations. The SAFT B-scan shown in Figure 2 is an example of a typical image from sound concrete. Selection of a damage free reference scan is possible based on past experience with signal interpretation of SAFT B-scans [27].

When possible, coring should be conducted to verify that the reference scan is indeed damage free.

There is generally little variation between B-scans of concrete in relatively good condition at different locations if the same instrument settings are used, while there is a significant variation between scans where flaws are present at different locations. Therefore, sound concrete will have the same level of correlation with the reference B-scan, whereas the correlation of scans with flaws at different locations will fluctuate. It should be noted that systematic flaws or inclusions (such as metal reinforcements) that extend horizontally at similar depths could potentially affect the reference scan selection. In these cases, as well as cases where the structural geometry is inconsistent within the scanning area, the current formulation of the 2D-UTSA method is not applicable.

The 2D-UTSA method requires selection of a reference B-scan based on engineering judgment, which raises concerns of sensitivity of the 2D-UTSA analysis to the choice of reference scan. To investigate this issue, a procedure for generating a reference scan was also introduced and used in the analysis. In this procedure, the reference scan is taken as the average of all of the B-scans in the set being compared. Because each B-scan has an intensity value associated with each pixel location, and the dimensions of matrices containing the intensity values is the same for all B-scans, the resulting reference scan associated with this procedure is simply the average intensity value for all pixel locations in the scanned area. It is expected that sound concrete may not necessarily have as high of a correlation with the generated reference scan as is the case for a manually selected reference scan. However, if a significant portion of measurements are made on sound concrete, the sound concrete locations should result in similar correlation values, while unsound concrete will result in lower values due to the randomness of flaws. Thus, decreases are still present in the correlogram even when the reference scan includes contributions from the flawed concrete

locations. Thus, this method is not overly sensitive to selection of the reference scan, and can be generally applied to locate areas of flawed concrete.

EXPERIMENTAL PROCEDURE

To evaluate the robustness of the 2D-UTSA method in identifying subsurface distresses, a series of tests were conducted. This included testing at the Minnesota Road Research Facility (MnROAD) [28] and the Federal Aviation Administration's National Airport Pavement Test Facility (NAPTF) [29].

The MIRA testing at MnROAD was conducted to verify the robustness of the MIRA 2D-UTSA method for locating defects with known dimensions and locations. To accomplish this, various defects were fabricated and embedded in the concrete at a fully bonded two-lift concrete pavement construction test site. The defects were fabricated to represent random "honeycombing" flaws in the concrete. The three defects embedded in the concrete included plastic wrapped aggregate in the center of the slab, a plastic wrapped porous concrete semi-cylinder on the left side of the slab, and a porous concrete semi-cylinder on the right side of the slab. Figure 4 shows the fabricated inclusions.

The testing involved 41 adjacent MIRA B-scans taken in 3 in. (76 mm) increments above the fabricated inclusions. After each scan, MIRA was moved three inches to the right, so that each adjacent B-scan is overlapping the previous B-scan along the length of MIRA (the horizontal axis of the B-scans). Using this type of testing procedure, it would be expected that the reflections from each of the embedded inclusions should move toward the left side of the B-scan as the device is moved to the right.

MIRA testing at the NAPTF was conducted to verify the 2D-UTSA technique in a situation where the presence or type of damage was unknown. Testing was conducted on a slab exposed to a potassium acetate deicer. As indicated in Fig. 5, cores taken at a location in

this slab prior to MIRA testing showed little to no damage. MIRA testing was conducted to verify that the “damage free” core was representative of the rest of the pavement. The testing procedure was similar to that conducted at MnROAD with 3 in. (76 mm) increments between adjacent scans. However, the scanning step size direction was perpendicular to the length of MIRA rather than along the length of MIRA.

EXPERIMENTAL RESULTS AND DISCUSSION

Identification of Fabricated Defects at MnROAD

The 2D-UTSA correlogram for MIRA scans taken at MnROAD locations without fabricated distresses are shown in Figure 6. It can be observed from this figure that there is a small amount of variation in Pearson’s coefficient at these locations, ranging from 0.90 to 0.93. This small scatter could be caused by structural noise from the variable aggregate and air void distribution. When analyzing the presence of flaws or inclusions in concrete, this type of scatter in Pearson’s coefficient should be ignored.

Figure 7 shows the 2D-UTSA correlogram of the B-scans obtained above of the artificial defects using a manually selected reference scan representing “damage free” concrete. Decreases in Pearson’s correlation can be observed in three locations that are much larger than that which would be expected from structural noise. These decreases in Pearson’s correlation coefficient correctly indicated the presence of the fabricated defects, and are similar to decreases in the IESA analysis of the simulated defects shown in Fig. 3.

A zoomed-in view of the leftmost artificial defect and corresponding correlogram dip, as well as sample SAFT B-scans resulting in the drop in Pearson’s correlation, are shown in Fig. 8. In this case, observations of the various B-scans indicate the presence of the distress by the reflection (dark area) at a shallower depth than the concrete thickness. Shadowing of the backwall reflection from the concrete-base interface below the artificial defect can also be

observed. While in this case the defect could be identified by visual inspection of the B-scan, use of the 2D-UTSA method mitigates this need for engineering judgment, and can be used as a more efficient and objective analysis method for larger scale cases where it is not feasible to manually evaluate each scan in detail. The MnROAD testing allowed for verification of the 2D-UTSA procedure with regard to identifying typical subsurface defects in preparation for applications where the presence, type, and location of any possible defects are unknown.

NAPTF Blind Test and Core Verification

The verified 2D-UTSA method was then applied to the NAPTF concrete pavement described in the “Experimental Procedure” section. A trend similar to that shown in Figure 6 was observed at most locations, confirming that the “damage free” cores were representative of most of the pavement area. However, in one location, a decrease in the Pearson’s correlation similar to that seen in Figures 3 and 8 was observed in the correlogram (see Figure 9). The SAFT B-scans adjacent to, as well as directly at the locations of decreased correlation, are shown in Figure 10. A shallow, approximately 4 in. (~100 mm) deep reflection can be observed in addition to shadowing of the backwall reflection at locations A through D corresponding to the dip in the correlogram. A core was taken at the location of the observed dip in the correlogram. Figure 9 shows the presence of a horizontal delamination, as well as some poor consolidation in the core. Forensic analysis of the cross-section of the core and pavement interface where the core was taken also identified that the delamination covered a smaller portion of the MIRA aperture at locations A and D from Figure 9, while locations B and C correspond to scans taken directly above the delamination. This verifies that the 2D-UTSA identification of a subsurface defect was indeed correct.

Generated Reference B-Scan Analysis

In this section the robustness of the 2D-UTSA method is evaluated by replacement of the manually selected reference B-scan with an averaged reference B-scans, as discussed previously. Figure 11 shows a correlogram created using the averaged reference scan representing the same MnROAD area shown in Figure 7. It can be observed that the use of the averaged reference scan results in lower correlations than those obtained from the manually selected reference scan. However, correlogram dips are observed at the same locations as in the correlogram generated using the manually selected reference scan. Thus, the 2D-UTSA analysis using the averaged reference scan method also resulted in detection of the fabricated defects.

The averaged reference scan approach was also applied for 2D-UTSA analysis on the NAPTF slab. Figure 12 shows the correlogram generated using the averaged reference scan for the same location where a subsurface defect was identified. This analysis was conducted in an area where 40 percent (4 of 10 scans) of the scans were taken in the vicinity of the subsurface defect. It can be observed that even in this challenging case, the decrease in the Pearson's correlation is observed when using the averaged reference scan. However, locations A and D were not identified as having any distresses below the scanning location. Therefore, even for a reference scan which is not completely representative of sound concrete, the 2D-UTSA analysis is capable of damage detection if a significant portion of the scans are taken on sound concrete. However, proper selection of the reference scan increases the resolution of 2D-UTSA analysis.

SUMMARY AND CONCLUSIONS

Previous laboratory studies and analytical modeling demonstrated that the IESA method is an effective tool for flaw detection using impact-echo signals. In this paper, the method

was generalized for use with ultrasonic tomography SAFT B-scans or with other tomographic reconstructions. The two-dimensional ultrasonic tomography signature analysis method (2D-UTSA) was developed for the analysis of concrete pavement with no systematic inclusions (i.e., reinforcement) and a constant geometry (i.e., thickness), when a majority of the scans are taken on sound concrete. The study involved evaluation of correlograms of individual scans using reference scans on sound concrete. The method was evaluated for identification of fabricated subsurface defects with known dimensions and locations. A blind test of the method showed 2D-UTSA to be capable of identifying naturally occurring subsurface defects, which was verified through coring.

An additional analysis involved replacement of the selected reference scan with a reference scan obtained by averaging all of the scans in the set. It was observed that, even for a reference scan which is not completely representative of sound concrete, the 2D-UTSA analysis is still capable of damage detection, if a significant portion of the scans are taken on sound concrete. However, proper selection of the reference scan increases the resolution of 2D-UTSA analysis. While the 2D-UTSA method was able to identify subsurface defects under the conditions of this study, the method should be modified for identification of extended planar flaws or for comparison of locations with differing structural geometries.

Although more field verification of the 2D-UTSA method should be conducted, the results of this study indicate that this method is an attractive tool for rapid subsurface damage detection in concrete structures such as pavements. Furthermore, use of the 2D-UTSA method mitigates the need for subjective engineering judgment in some cases, and can be used as a more efficient and objective analysis method for larger scale tests where it is not feasible to evaluate each scan in detail. The 2D-UTSA procedure is especially useful in applications where the presence, type, and location of any possible defects are unknown.

ACKNOWLEDGMENTS

The research described in this paper was conducted as part of a joint Federal Highway Administration (FHWA) and Minnesota Department of Transportation (Mn/DOT) project overseen by Mr. Tom Yu and Dr. Shongtao Dai. Mr. Chuck Teubert and Mr. Josh Davis from SRA, Inc. were instrumental in the Federal Aviation Administration NAPTF testing and forensic analysis. Tim Clyne and Luke Johanneck from Mn/DOT also contributed in the MnROAD testing.

REFERENCES

- [1] Gucunski N., Romero F., Kruschwitz S., Feldmann R., Abu-Hawash A., Dunn M., "Multiple Complementary Nondestructive Evaluation Technologies for Condition Assessment of Concrete Bridge Decks." *Transportation Research Record: Journal of the Transportation Research Board of the National Academies*. Volume 2201. Pages 34-44. 2010. Online Date: Wednesday, December 01, 2010.
- [2] Chen, D H, Nazarian, S; Bilyeu J. "Failure Analysis of a Bridge Embankment with Cracked Approach Slabs and Leaking Sand." *Journal of Performance of Constructed Facilities*. American Society of Civil Engineers. 21.5 (September 2007):375.
- [3] Li, J., Zollinger, D.G., Lytton, R.L., "Detection of Delamination in Concrete Pavements Using Ground-Coupled Ground-Penetrating Radar Technique." *Transportation Research Record: Journal of the Transportation Research Board*, Volume 2087 / 2008, pp. 68-77, 2008
- [4] Maierhofer C., "Nondestructive Evaluation of Concrete Infrastructure with Ground Penetrating Radar." Federal Institute for Materials Research and Testing (BAM) Berlin, Germany. *Journal of Materials in Civil Engineering*. ASCE. Volume 15, Issue 3, Issue Date: May/June 2003, pp. 287-297.
- [5] Chong K. P., Carino N.J., and Washer G., "Health monitoring of civil infrastructures." National Science Foundation, National Institute of Standards and Technology, and the Federal Highway Administration. Institute of Physics Publishing. *Smart Materials and Structures* PII: S0964-1726(03)61742-8, Date: 2003, pages 483-493
- [6] Rao, S. Hoegh, K. Yu, H.T. Khazanovich, L. "Evaluation of Dowel Alignment Constructability in Portland Cement Concrete Pavements." *Transportation research record Journal of the Transportation Research Board*, Washington D.C. 2098.-1 (2009):86.
- [7] Hoegh, K., T. Yu, and L. Khazanovich, "MIT SCAN Application in North America-Five Years After." *Proceeding of the Ninth International Conference on Concrete Pavements*, 450-462, San Francisco, CA, USA, 2008.
- [8] Hossain, S., Elfino, M.K., "Field Demonstration of Magnetic Tomography Technology for Determination of Dowel Bar Position in Concrete Pavement." *VTRC 06-R40*, Virginia Transportation Research Council, June 2006.
- [9] Washer, G., Fenwick R., Bolleni N., and Harper J. "Effects of Environmental Variables on Infrared Imaging of Subsurface Features of Concrete Bridges." *Journal Transportation Research Record: Journal of the Transportation Research Board*. Publisher: Transportation Research Board of the National Academies. Volume 2108. 2009. Pages 107-114.
- [10] Clark, M. R., D. M. McCann, and M. C. Forde. "Application of Infrared Thermography to the Non-Destructive Testing of Concrete and Masonry Bridges." *NDT and E International*, Vol. 36, No 4, 2003, pp. 265-275.

- [11] Maser, K. R., and W. M. K. Roddis. "Principles of Thermography and Radar for Bridge Deck Assessment." *Journal of Transportation Engineering*, Vol. 116, No. 5, 1990, pp. 583–601.
- [12] Rose J.L. (Author), "Ultrasonic Waves in Solid Media." *Journal of Acoustical Society of America*. Volume 107, Issue 4, pp. 1807-1808. April 2000.
- [13] Liu T., Zhou J., Osterman K.S., et al. "Measurements of radiation-induced skin changes in breast-cancer radiation therapy using ultrasonic imaging." *Proceedings of the 2008 IEEE International Conference on BioMedical Engineering and Informatics 2008*; 2:718–722.
- [14] Schubert, Frank and Köhler, Bernd. "Three-Dimensional Time Domain Modeling of Ultrasonic Wave Propagation." *Fraunhofer Institute for Nondestructive Testing, Dresden Germany. Journal of Computational Acoustics (2001). IMACS*. pp. 1543-1560.
- [15] Schubert, F. and Kohler B., "Ten Lectures on Impact-Echo." *Journal of Nondestructive Evaluation. Special Issue: Acoustic and Electromagnetic Nondestructive Evaluation of Concrete Structures*. Volume 27, Date: 2008. Pages 1-3, 5-21
- [16] Carino, N.J., "The Impact-Echo Method: An Overview," *Proceedings of the 2001 Structures Congress & Exposition, May 21-23, 2001, Washington, D.C., American Society of Civil Engineers, Reston, Virginia, Peter C. Chang, Editor, 2001*.
- [17] Zhu, J. "Imaging Concrete Structures Using Air-Coupled Impact-Echo." *Dissertation submitted in partial fulfillment of Ph.D. in Civil and Environmental Engineering at the University of Illinois at Urbana-Champaign, 2005*.
- [18] Gibson, A. and Popovics J.S. "Lamb Wave Basis for Impact-Echo Method Analysis." *Journal of Engineering Mechanics*. Volume 131 Issue 4. (2005). *American Society of Civil Engineering*. (6 pages).
- [19] Zhu, J. and Popovics, J. S. "Non-contact imaging for surface-opening cracks in concrete with air-coupled sensors." *Materials and Structures*. Volume 38, Issue 9. (2005). *Springer Netherlands* pages 801-806.
- [20] Shevaldykin, V. G., Samokrutov A. A., and Kozlov V. N., "Ultrasonic Low-Frequency Transducers with Dry Dot Contact and Their Applications for Evaluation of Concrete Structures." *IEEE Ultrasonics Symposium Proceedings 1 & 2*, 793–798. (2002)
- [21] Mayer, Klause et al. "Characterization of Reflector Types by Phase-Sensitive Ultrasonic Data Processing and Imaging." *Journal of Nondestructive Evaluation (2008)*. *Springer Science*. Pp. 35-45.
- [22] Nesvijski, E.G., "On the Problem of Application of the Conic and Exponential Wave Guiding Extensions for Ultrasonic Transducers for Materials Testing". *Journal: NASTA Technical Bulletin, Philadelphia, PA, USA, 1997 (ISSN 1079-8498), Volume 3*, pp. 49-56.

- [23] Khazanovich, L., R. Velasquez, and E. Nesvijski. "Evaluation of Top-Down Cracks in Asphalt Pavements Using a Self-Calibrating Ultrasonic Technique" (2005) Transportation Research Record: Journal of the Transportation Research Board, No. 1940, pp. 63–68.
- [24] Marklein, R. et al. "Linear and Nonlinear Inversion Algorithms Applied in Nondestructive Evaluation." Inverse Problems (2002). Inst. of Physics Publishing.
- [25] Langenberg, K.J. et al. "Inverse Scattering with Acoustic, Electromagnetic, and Elastic Waves as Applied in Nondestructive Evaluation." Chapter 2 in Wavefield Inversion. (CISM) International Centre for Mechanical Sciences, Edited by Armand Wirgin (2001).
- [26] Acoustic Control Systems (ACSYS) – Devices for non destructive testing of metals, plastics and concrete, MIRA - Ultrasonic Tomograph for Imaging of Concrete Structures Ref. No: 1025, <http://acsys.ru/eng/> (accessed February 2010), 2008.
- [27] Hoegh K., Khazanovich L., Yu H.T. "Ultrasonic Tomography Technique for Evaluation of Concrete Pavements." Transportation Research Record: Journal of the Transportation Research Board, No. 2232, pp. 85–94. 2011.
- [28] Tompkins D., Khazanovich L., Johnson D.M. "Benefits of the Minnesota Road Research Project." Transportation Research Record: Journal of the Transportation Research Board of the National Academies. Volume 2087 / 2008. 12-19. Online Date: January 22, 2009
- [29] Guo E. H., Hayhoe G. F., and Brill, D. R. "Analysis of NAPTF Traffic Test Data for the First-Year Rigid Pavement Tests Items." FAA Airport Technology Transfer Conference. Atlantic City, New Jersey, USA. 2002.

LIST OF FIGURES

Figure 1. MIRA ultrasonic tomography device and comparison with traditional impact echo method [17, 24].

Figure 2. Representative B-scan of PCC pavement in good condition.

Figure 3. Example of an impact-echo correlogram based on Pearson's Correlation Coefficient [17].

Figure 4. Fabricated inclusions: (a) a plastic-wrapped porous concrete semi-cylinder, (b) plastic-wrapped aggregate, and (c) a porous concrete semi-cylinder.

Figure 5. Core indicating "damage free" concrete at the NAPTF slab location.

Figure 6. Correllelogram of concrete without an embedded inclusion, indicating the absence of a subsurface defect.

Figure 7. Correlogram from 41 adjacent measurements above the fabricated distresses.

Figure 8. Zoomed-in view of the leftmost fabricated defect, corresponding dip in the correlogram, and sample B-scans indicating the presence of the defect.

Figure 9. Correlogram indicating a subsurface defect at the NAPTF site using a manually selected reference scan.

Figure 10. SAFT B-scans at locations A,B,C,D as shown in Figure 9.

Figure 11. Correlograms from 41 adjacent measurements above the fabricated distresses using the averaged reference scan.

Figure 12. Correlogram indicating subsurface defect at the NAPTF test slab, as compared to the averaged reference scan.

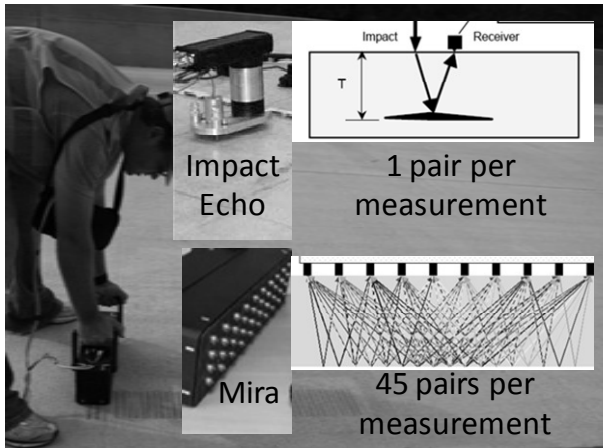


Figure 1

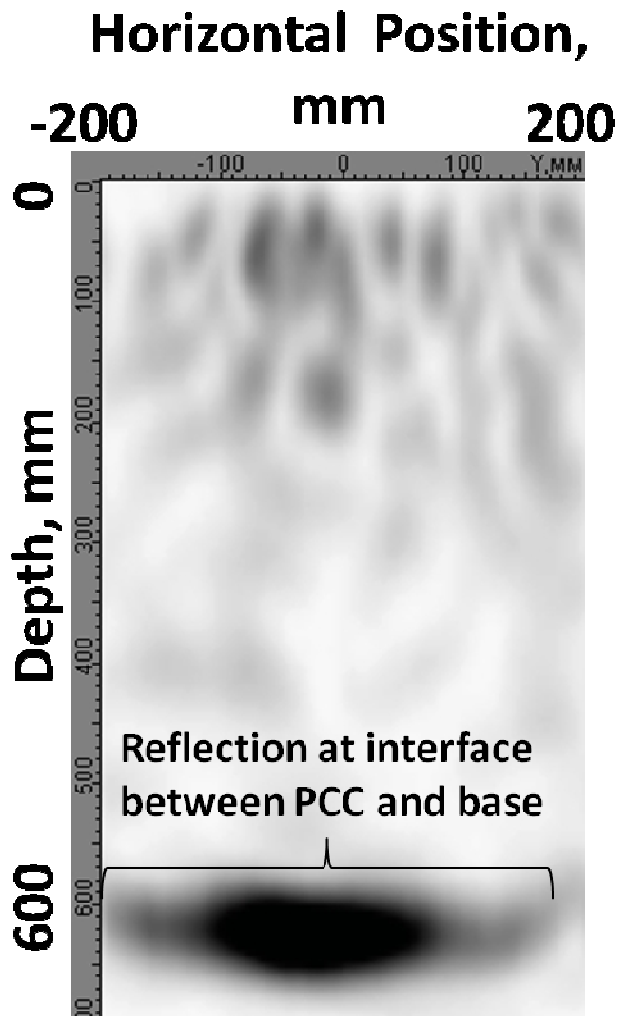


Figure 2

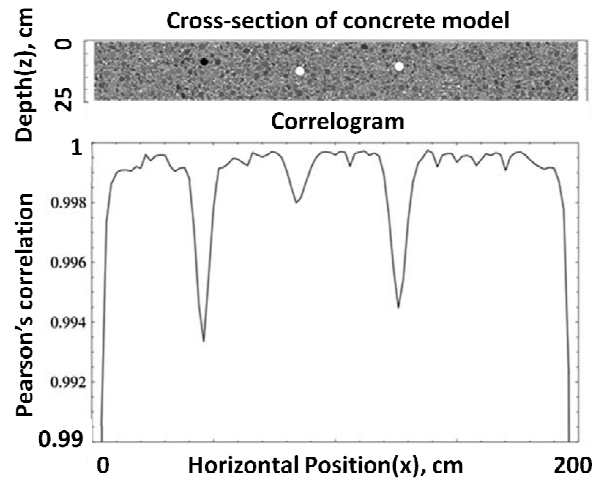


Figure 3

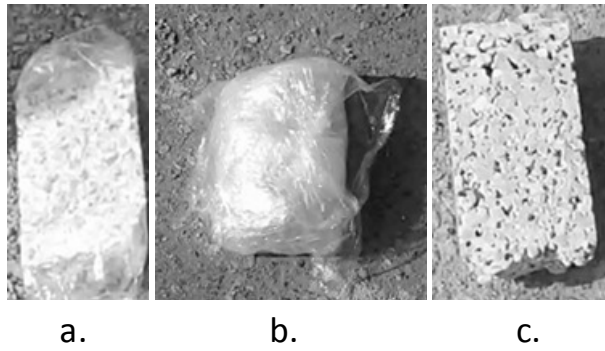


Figure 4

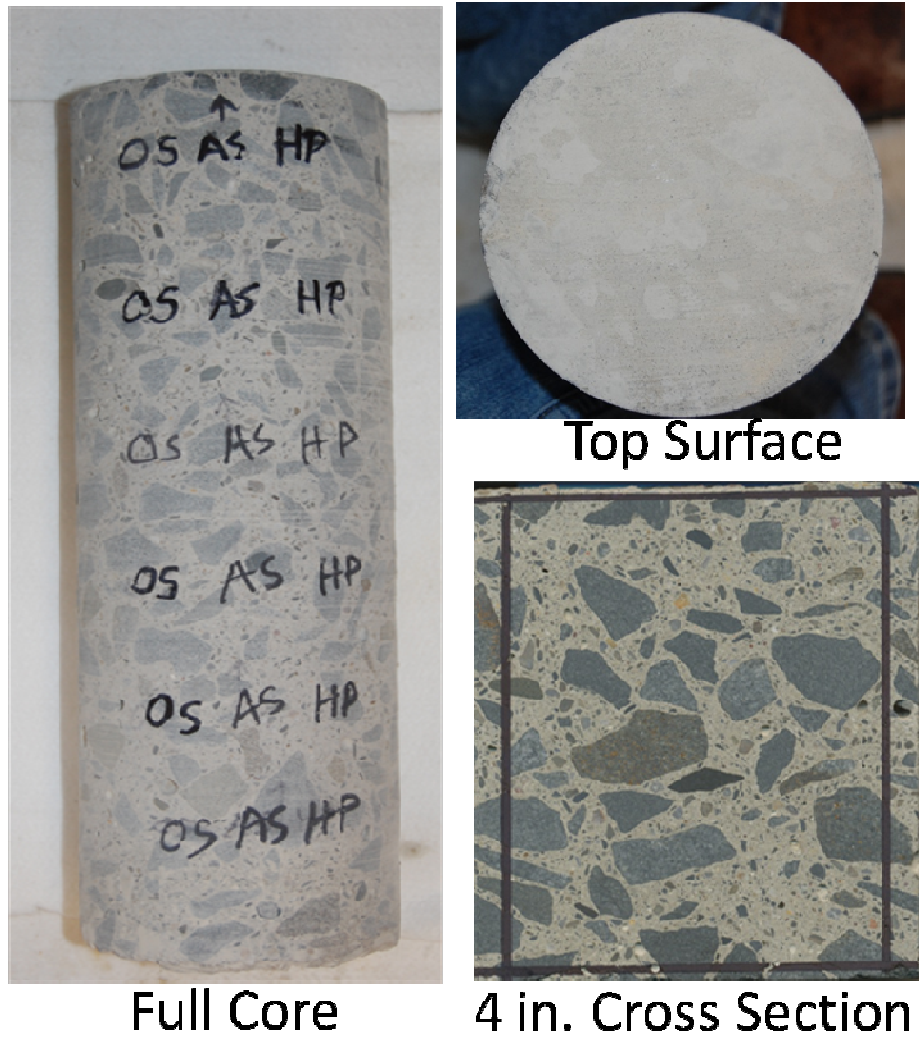


Figure 5

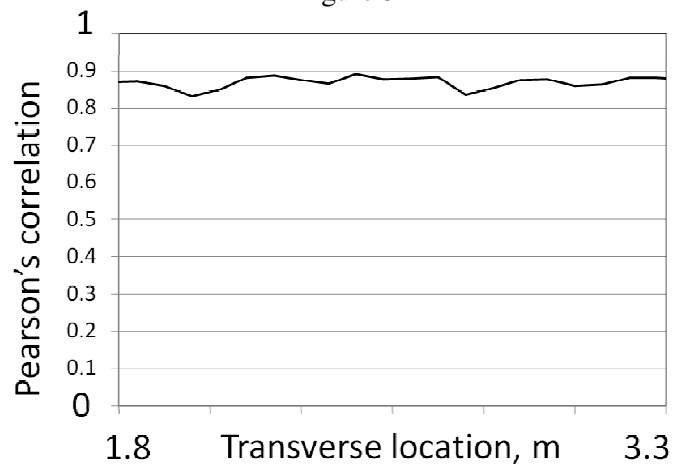


Figure 6

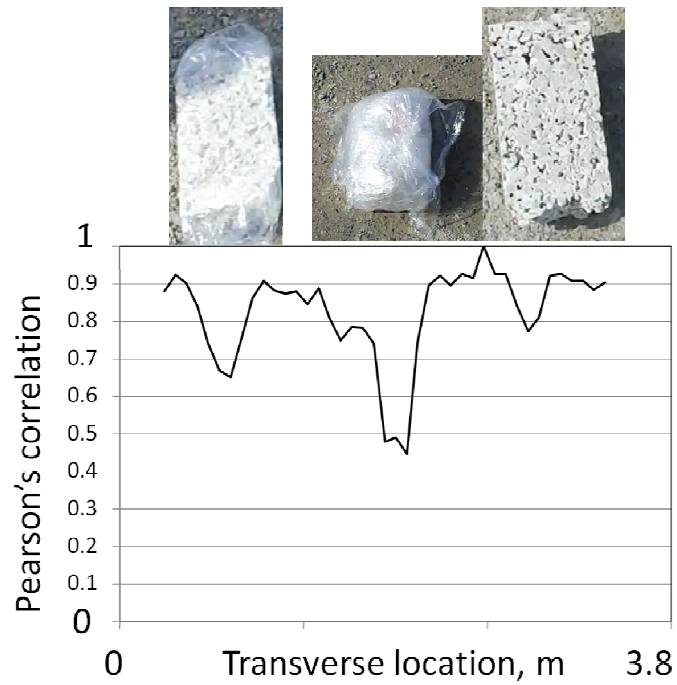


Figure 7

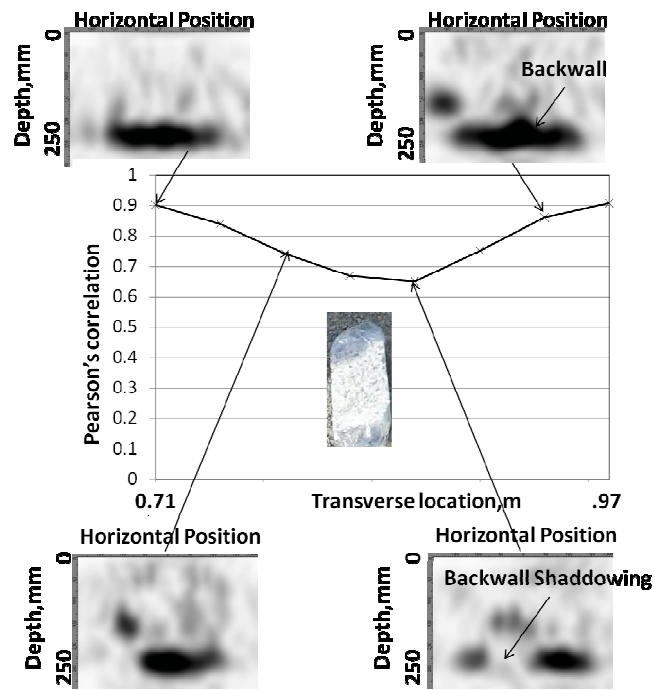


Figure 8

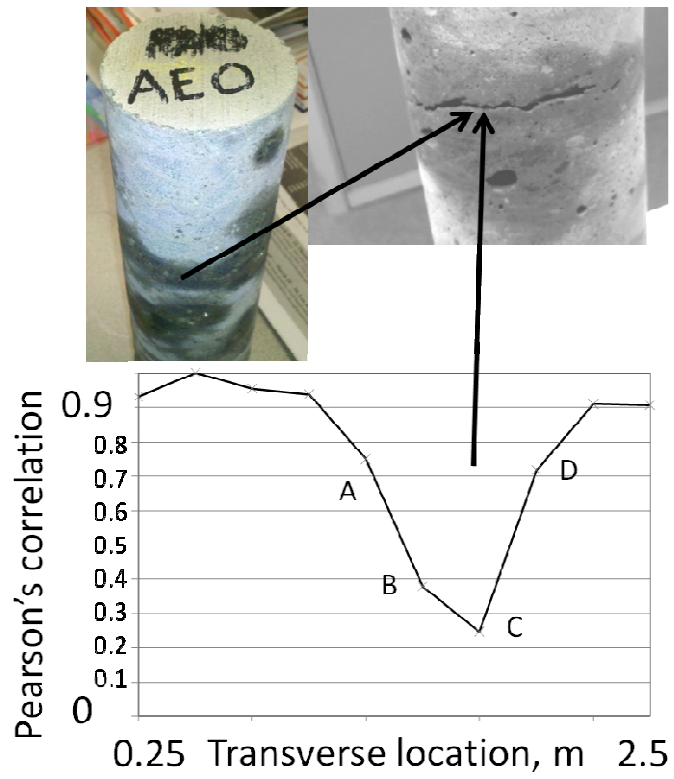


Figure 9

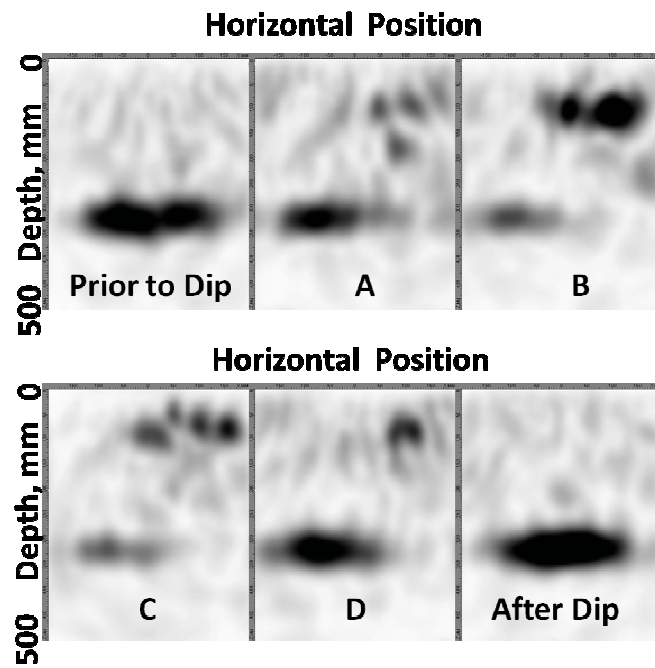


Figure 10

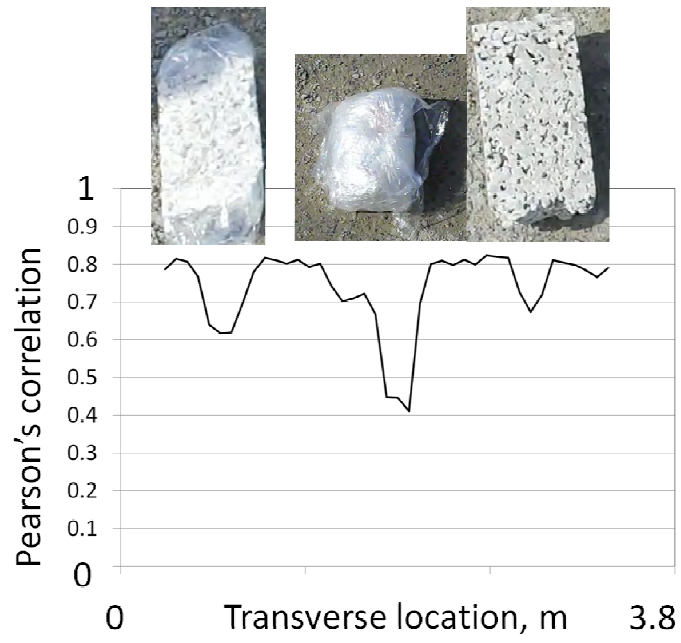


Figure 11

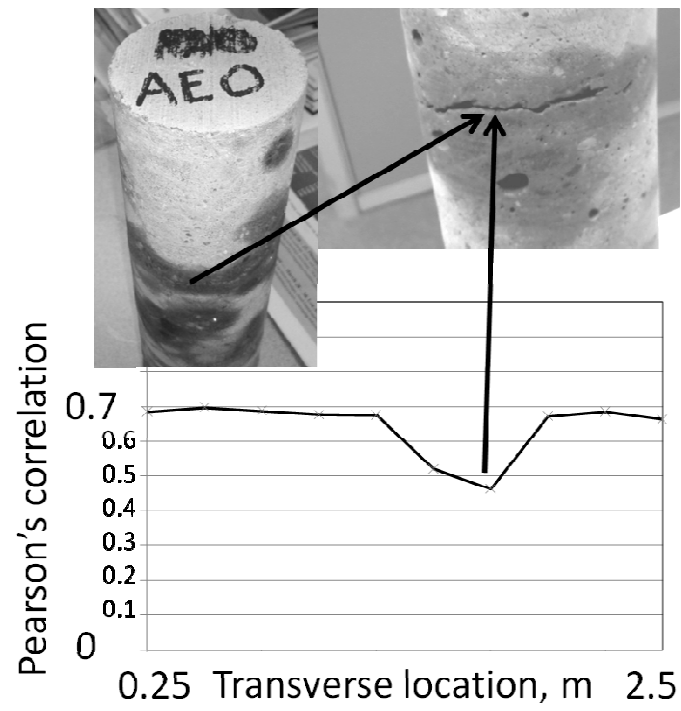


Figure 12